Dynamically Tunable Deep Subwavelength High-Order Anomalous Reflection Using Graphene Metasurfaces

Chao Wang, Wenwei Liu, Zhancheng Li, Hua Cheng, Zhi Li, Shuqi Chen,* and Jianguo Tian

Graphene-based metasurfaces have emerged as promising photoelectric devices that can dynamically control the behavior of electromagnetic waves. The high-order anomalous reflection provides an additional degree of freedom in the field of photonic research. Here, a series of gradient graphene metasurfaces with high-order modes to manipulate the wavefront of reflected light is proposed. By properly arranging the graphene nanostructures, 5-order anomalous reflection and 15-order high-quality Laguerre–Gaussian beams are achieved. Furthermore, the efficiency of the metasurfaces is dynamically controlled by tuning the electrostatic gating to change the Fermi energy of graphene. This work offers a new idea for the development of tunable wavefront-controlling devices and contributes to a wide range of applications in photonic systems.

Metasurfaces are a new class of metamaterials that provide fascinating capabilities for manipulating light in an ultrathin platform. Compared with 3D bulk metamaterials, metasurfaces are able to deeply modify the wavefront of electromagnetic waves, and its ultrathin thickness helps to reduce nonignorable energy losses.[1,2] By properly engineering the geometry of the nanostructures on metasurfaces, many novel phenomena have been explored using plasmonic metasurfaces, for instance, Hall effect,[3] full control of polarization,[4] and nonlinear phase control.[5,6] Metasurfaces can control the optical phase, amplitude, and polarization of transmitted or reflected light at the nanoscale, capable of achieving the phase variation covering 2π range without sacrificing the uniformity of amplitude. There are two primary methods to attain phase modulation at the nanoscale: one is suitably tailoring the structure of nanoparticles such as V-shaped antennas, the abrupt phase changes could be introduced.[7] Another is utilizing the Pancharatnam–Berry phase to construct a discontinuous phase profile by varying the orientations of nanoantennas.[8] Through designing

the space-variant nanoantennas, many researchers have realized beam steering, such as vortex beams,[9,10] Bessel beams,[11] Airy beams,[12] and manipulating optical orbital angular momentum.[13] Recently, the development of a feasible device that can dynamically tune the light characteristics has gradually attracted enormous interests. Using graphene-loaded plasmonic metasurfaces, tunable broadband anomalous refraction,[14] efficient controls of the Goos–Hänchen shift,[15] and optical polarization encoding[16] have also been realized. However, most of these research studies are working in the −1 to 1 order of diffraction modes. Li et al. manipulated the wavefront of light by gold antennas metasurfaces with three-order modes.[17] Although the phase shift is larger than 2π, the phase shift and the scattering amplitude depend on the design of structures, which can hardly be dynamically controlled. Due to the difference in electrical conductivity between metal and graphene, metallic metasurfaces are difficult to achieve ultra-high-order anomalous reflection or refraction.

Many researchers have focused on achieving tunable and switchable metasurfaces.[18] Traditional dynamically tuning methods are based on thermal or mechanical mechanism, which are usually limited by slow response speed or small adjustable range.[19,20] Graphene, as a monolayer of hexagonally arranged carbon atoms, has attracted tremendous attention for its extraordinary performance. The optical conductivity of graphene can be effectively tuned by electrochemical potential via electrostatic gating.[21] At the near-infrared and mid-infrared wavelengths, graphene metasurfaces have shown the electro-optical responses. For example, large phase differences could be accomplished by integrating single-layer graphene with metasurfaces.[22] Graphene nanoresonators could support multiple plasmonic resonances that interact with mid-infrared light.[23] Graphene split ring resonators could enhance infrared extinction and absorption.[24] The combination of monolayer graphene and metasurface could produce a strong Fano resonance, which may benefit applications in sensing.[25] The graphene metasurfaces that could work at different wavebands can be independently tuned by electrically controlling the Fermi energy of corresponding graphene layers.[26] On the other hand, the lattice size of a metasurface should be small enough to meet the Nyquist sampling criterion ($P < 1/2F_m$, where F_m is the maximum spatial Fourier frequency of the metasurface).

Dr. C. Wang, Dr. W. Liu, Dr. Z. Li, Prof. H. Cheng, Dr. Z. Li, Prof. S. Chen, Prof. J. Tian
Laboratory of Weak Light Nonlinear Photonics
Ministry of Education
School of Physics, Teda Applied Physics Institute
Nankai University
Tianjin 300071, China
E-mail: schen@nankai.edu.cn

The ORCID identification number(s) for the author(s) of this article can be found under https://doi.org/10.1002/adom.201701047.

ADVANCED
SCIENCE NEWS
www.advancedsciencenews.com

ADVANCED
OPTICAL
MATERIALS
www.advopticalmat.de

For a complicated or rapidly varied phase distribution, a deep subwavelength nanostructure is needed to realize the required phase modulation. As demonstrated in the following part, for graphene-based metasurfaces, the size of the nanostructure can decrease to ~λ/80 in infrared waveband; whereas for traditional plasmonic or dielectric metasurfaces, the size of the nanostructures is around λ/8 to λ/3.[27–29] This characteristic makes graphene possible to support a much higher phase gradient, which enables graphene to be an excellent candidate for modulating the wavefront of electromagnetic waves and helps to improve the efficiency of holography, multifunctional imaging, and surface wave manipulation.

In this paper, we propose a tunable broadband anomalous reflective metasurface composed of periodically patterned graphene nanocrosses to control the wavefront of circularly polarized light in high-order modes. We demonstrate that the gradient metasurfaces can achieve a great phase shift up to $5 \times 2\pi$. In order to more intuitively show the high-order mode manipulation of the wavefront, we further build a series of space-variant metasurfaces based on the designed unit cells to realize high-order optical vector beams with high quality. The new degree of freedom enabled by the high-order modes facilitates the manipulation of wavefront and will promote more applications in nanophotonic systems.

Considering a linearly varied phase shift $\Phi(x)$ along the surface of a metasurface, the reflected or refracted wave can be steered. The Snell's law is modified in the generalized version[30]

$$n_o \sin\theta_o - n_i \sin\theta_i = \frac{\lambda}{2\pi}\frac{\mathrm{d}\Phi(x)}{\mathrm{d}x} \tag{1}$$

where θ_i and θ_o are the angles of the incident and refracted/reflected waves; n_i and n_o are the refractive indices of the input and output media, respectively. For reflection, the generalized Snell's law can be expressed as

$$\sin\theta_r - \sin\theta_i = \frac{\lambda}{2\pi n_i}\frac{\mathrm{d}\Phi(x)}{\mathrm{d}x} \tag{2}$$

where θ_r is the angle of the reflected waves. An accurate method to control $\Phi(x)$ is to use Pancharatnam–Berry phase with $\Phi(x) = 2\sigma\varphi$ for the anomalous light,[29] where φ is the orientation angle of the nanostructure, and $\sigma = \pm1$ is for left circularly polarized (LCP)/right circularly polarized (RCP) incident light. On the other hand, metasurfaces with a periodic phase shift can also be considered as a reflection grating, the equation of which can be expressed as[30]

$$\sin\theta_r - \sin\theta_i = m\frac{\lambda}{n_i P} \tag{3}$$

where P is period of the grating, and integer m is the order of reflection. When $\Phi(x)$ varies linearly by $m \times 2\pi$ over a distance P,
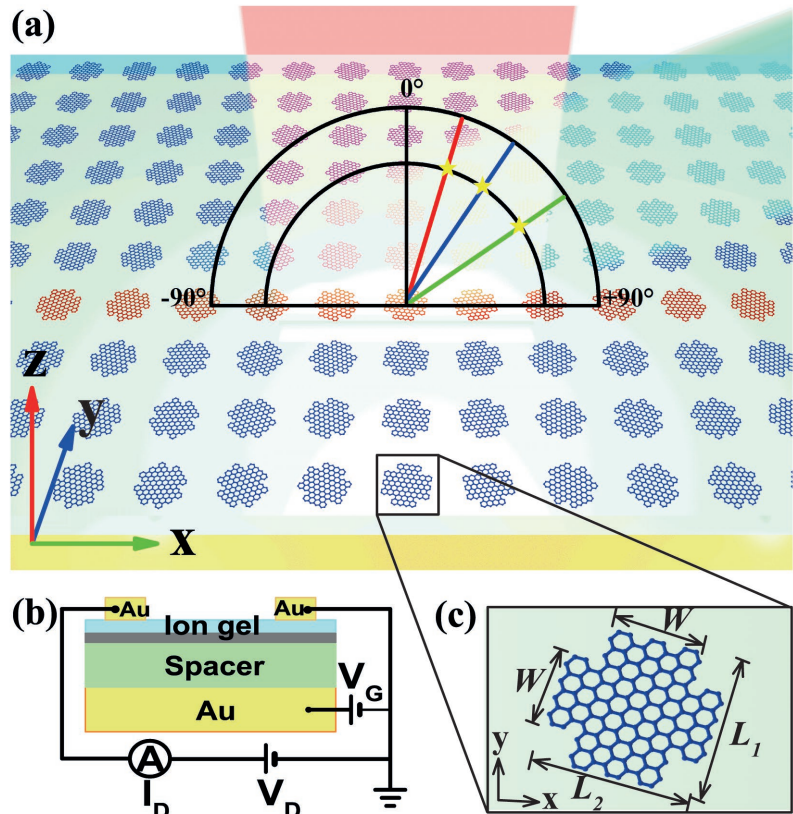

Figure 1. a) Schematic view of a reflective graphene nanocrosses metasurface. The thicknesses of ion gel and the middle spacer layer are 100 and 1500 nm. b) Cross section of ion gel-gated graphene transistors. c) Sketch of a single nanocross, $L_1 = 110$ nm, $L_2 = 105$ nm, $W = 80$ nm, and $S = 600$ nm (the distance between adjacent nanocrosses). The angle between one arm of nanocross (along L_1) and x-axis is defined as rotation angle φ.

we can obtain $\frac{\mathrm{d}\Phi(x)}{\mathrm{d}x} = \frac{2m\pi}{P}$ by combining Equations (2) and (3). In this study, we employ $m \times 2\pi$ rather than a wrapped phase range $[0, 2\pi)$ to characterize the ability to manipulate the wavefront of electromagnetic waves, just as described by the equation of grating $k_0 d\sin\theta = 2m\pi$.

We adopt the patterned array of graphene nanocrosses on a gold film to manipulate the wavefront of anomalous reflection in high-order modes, as shown in **Figure 1**. It consists of a ground gold plane and graphene nanocrosses, separated by a spacer with refractive index of 1.4. The thicknesses of ion gel and the middle spacer layer are 100 and 1500 nm, respectively. The optical constants of gold at mid-infrared regime are taken from ref. [31]. On the top of the graphene lies a layer of ion gel (Figure 1b), which serves as gate dielectric with high capacitance in graphene transistors.[32–34] The ion gel layer is described by a nondispersive permittivity: $\varepsilon = 1.82$.[34] Figure 1c shows the geometry parameters of a single graphene nanocross. The conductivity of graphene is computed within the local random phase approximation limit at zero temperature[21]

$$\sigma(\omega) = \frac{e^2 E_F}{\pi\hbar^2}\frac{i}{\omega + i\tau^{-1}} + \frac{e^2}{4\hbar}\left[\theta(\hbar\omega - 2E_F) + \frac{i}{\pi}\left|\frac{\hbar\omega - 2E_F}{\hbar\omega + 2E_F}\right|\right] \tag{4}$$

**ADVANCED
SCIENCE NEWS**
www.advancedsciencenews.com

**ADVANCED
OPTICAL
MATERIALS**
www.advopticalmat.de

here, $\tau = \mu E_F / e v_F^2$ is intrinsic relaxation time; $v_F \approx c/300$ is the Fermi velocity; and $\mu = 10000$ cm^2 Vs^{-1} is the measured DC mobility. The finite element method-based COMSOL Multiphysics software[35] was used to design and optimize the metasurfaces. For experimental characterization, the proposed graphene metasurfaces can be fabricated through commercial techniques of ion-beam sputter deposition and electro-beam lithography. The top-gate electrodes can be evaporated thermally through shadow masks.[32]

The designed tunable high-order anomalous refraction metasurfaces work in the reflection mode as the transmission is suppressed by the ground gold plane. We calculated the reflection of the graphene nanocross with the rotation angle of $\varphi = 90°$ under LCP light incidence. We optimized the geometric parameters with COMSOL to realize efficiency of the anomalous reflection as high as possible, with phase shift covering $-\pi$ to π. The spectral distance of response peaks will increase with decreasing of L_2, as shown in **Figure 2**a. It is worth mentioning that the difference between L_1 and L_2 is necessary because a C4-symmetry structure will show the same responses

when electromagnetic waves propagate along x and y directions, leading to no generation of the anomalous reflection. The reflection resonance has a blueshift as increasing of the width W, as shown in Figure 2b, where the Fermi energy is fixed at 0.9 eV. Considering both the response band and the reflection efficiency, we chose the optimized structural parameters, whose reflection spectrum is indicated by the red line in the Figure 2a. There are two distinct resonant peaks at the wavelengths of 8.31 and 8.60 μm. The origin of the resonances can be attributed to the electric dipole modes coupled to the propagating light, as shown in Figure 2d,e. The simulated near-field E_z shows that the surface plasmons in graphene are efficiently excited at two resonant wavelengths. Since the shorter wavelength can help to avoid the formation of evanescent wave, we chose the wavelength of 8.31 μm to further analyze the optical steering characteristics of an individual graphene nanocross. Figure 2c shows the amplitudes of anomalous reflection and the corresponding phase shifts for the individual graphene nanocross at the wavelength of 8.31 μm, where the Fermi energy is also fixed at 0.9 eV. Apparently, each nanocross has basically the same amplitude
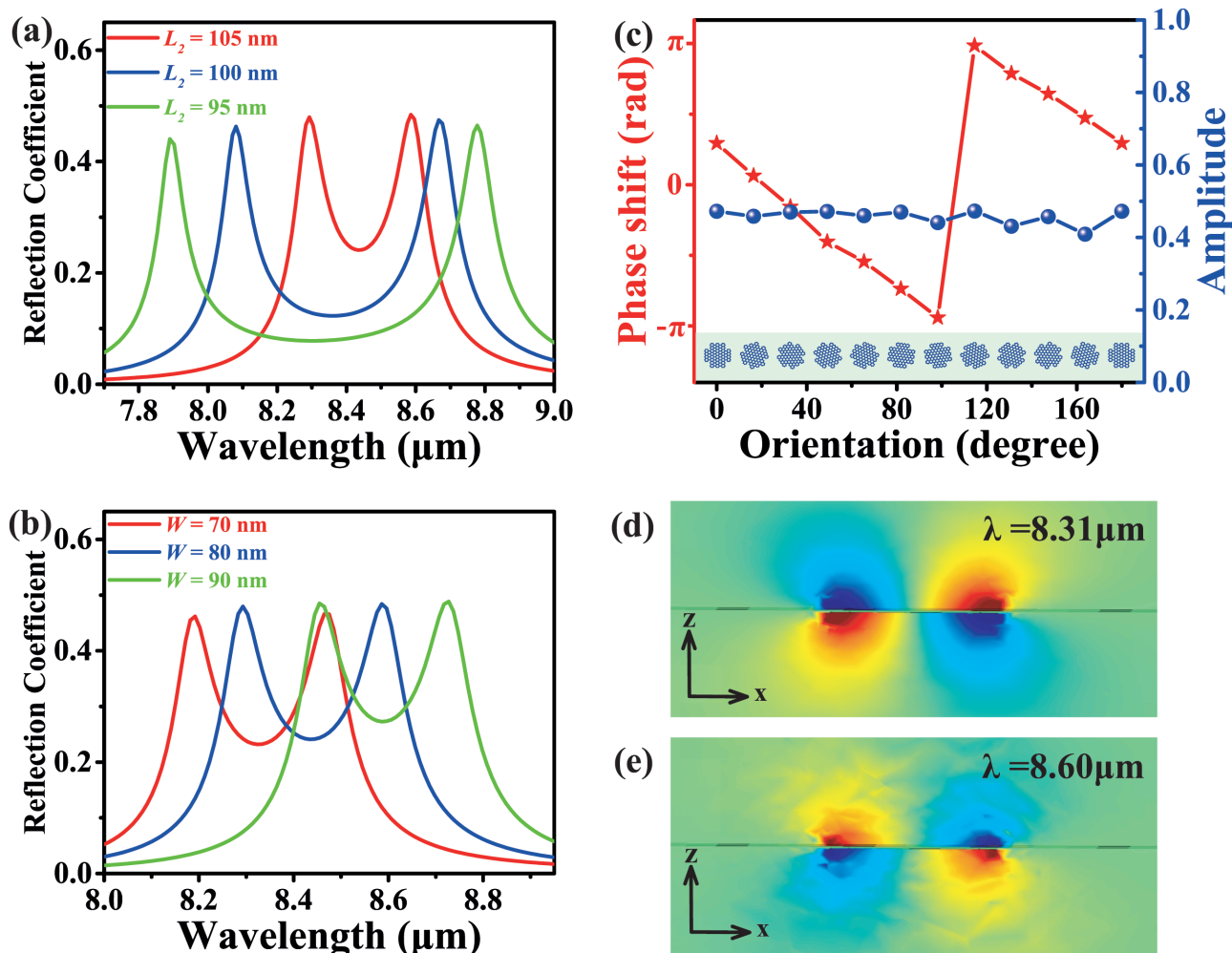

Figure 2. Simulated anomalous reflection spectra of the nanocrosses with varied length of a) L_2 and b) W, with the rotation angle $\varphi = 90°$. c) Amplitude and phase of the anomalous light with the rotation angle of the graphene nanocross changing from 0° to 180°. The electric near-field z component in the x–z plane (middle cut plane of the nanocross) at wavelengths of d) 8.31 μm and e) 8.60 μm. (c–e) were simulated with $L_2 = 105$ nm, $W = 80$ nm.

**ADVANCED
SCIENCE NEWS**

www.advancedsciencenews.com

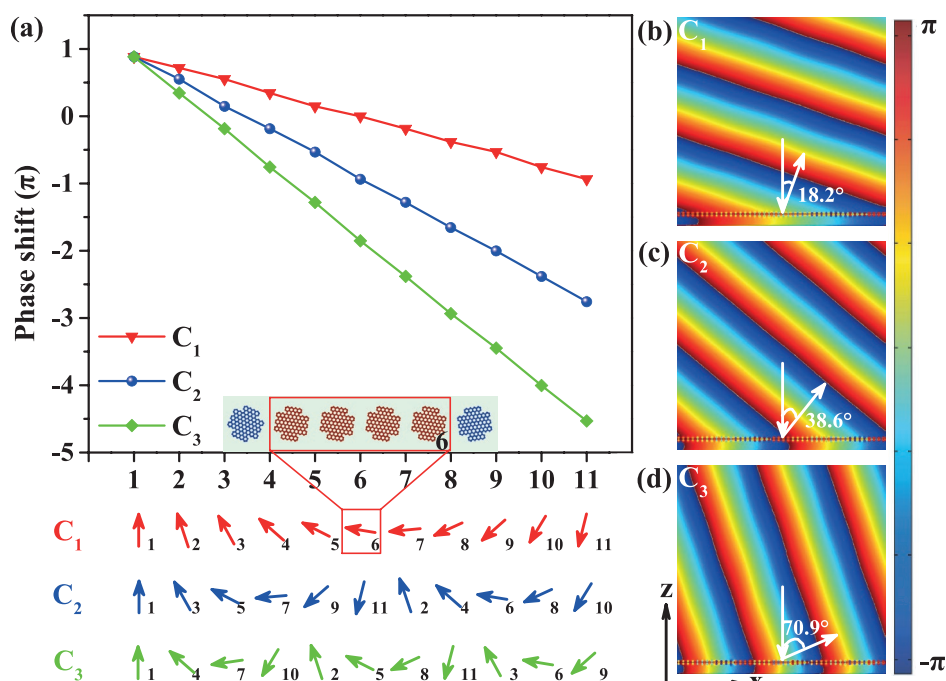**ADVANCED
OPTICAL
MATERIALS**

www.advopticalmat.de

Figure 3. a) Reflective phase shift for three arrangement modes of super cells. The arrows represent the rotation angles of the unit groups. The first row C_1 provides a total phase coverage of 2π, C_2 and C_3 extend the coverage to $2 \times 2\pi$ and $3 \times 2\pi$ with different arrangements of the selected 11 nanocrosses. Simulated phase distributions with structures in b) C_1, c) C_2, and d) C_3 of reflected LCP light under RCP incidence.

with a high-amplitude conversion efficiency and an entire phase range covering from 0 to 2π.

We changed the arrangement of the nanocrosses to obtain three orders of phase conversion. As shown in **Figure 3**a, the graphene super cell includes 11 unit groups, and each unit group has N graphene nanocrosses with same geometry and rotation angle (here, we set N as 4). The key point is that the graphene-based nanocross is far smaller than the working wavelength (about $\lambda/80$), which supports a light manipulation in extra subwavelength scale. The orientations of adjacent unit groups have a constant step of $m \times \pi/11$ in the x-direction. Then the period of the super cell is $P = 11 \times N \times S$, and the phase gradient is determined according to the formula $\dfrac{\mathrm{d}\Phi(x)}{\mathrm{d}x} = \dfrac{2m\pi}{P}$. The first row C_1 in Figure 3a is a common anomalous reflection array working in the fundamental mode. The adjacent
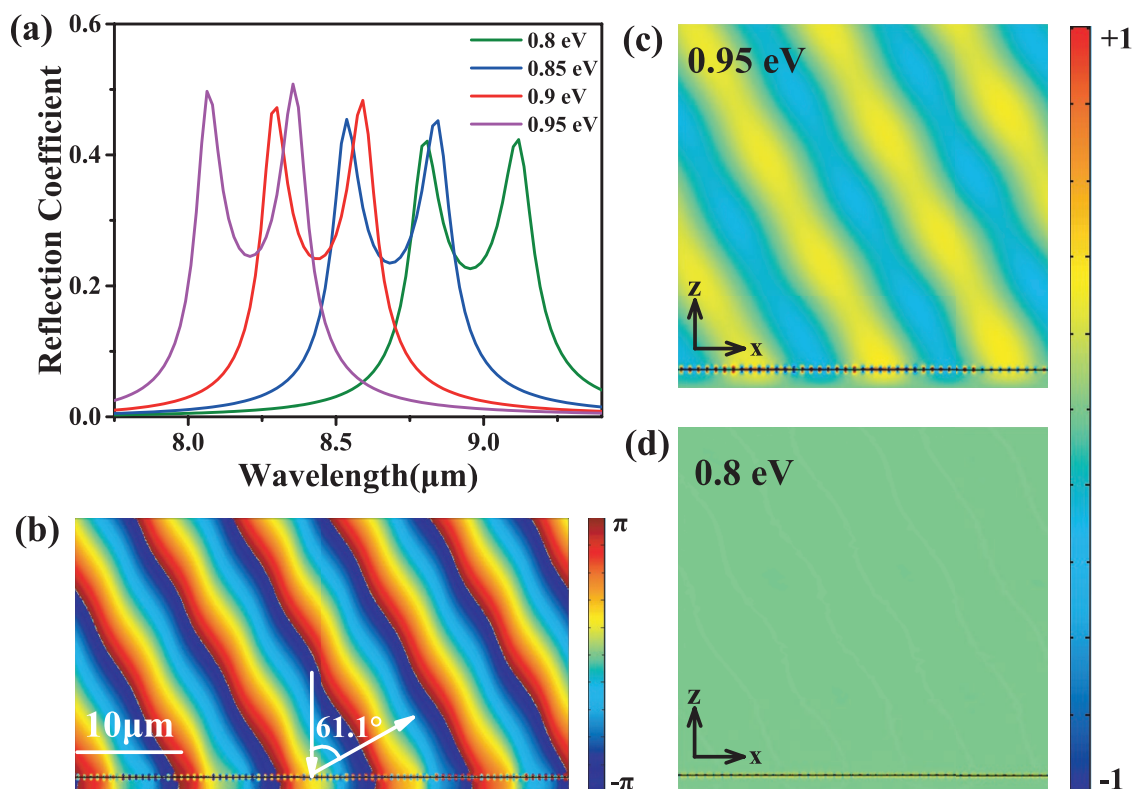

Figure 4. a) Simulated reflection amplitude spectra for a single graphene nanocross with different Fermi energy. b) Simulated phase distributions of five-order anomalous reflection. The electric anomalous component in the x–z plane at the Fermi energy of c) 0.95 eV and d) 0.8 eV.

ADVANCED
SCIENCE NEWS
www.advancedsciencenews.com

ADVANCED
OPTICAL
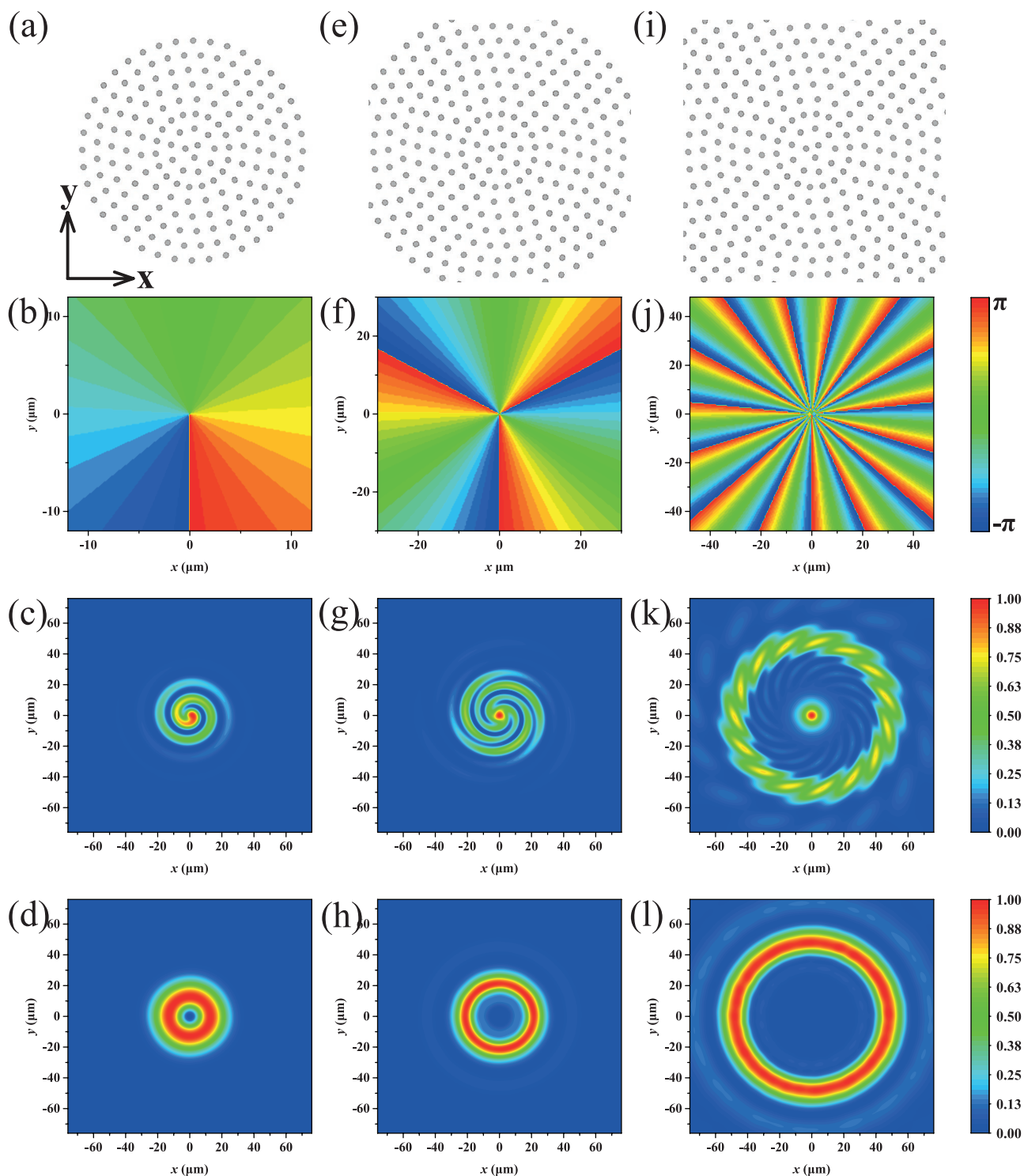MATERIALS
www.advopticalmat.de

Figure 5. Schematic models of the vortex-beam-generating metasurfaces for a–d) $m = 1$; e–h) $m = 3$; i–l) $m = 15$. Panels (a), (e), and (i) illustrate the structural distribution of the metasurfaces. Panels (b), (f), and (j) are the phase distribution for the corresponding metasurfaces. (c), (g), and (k) are the electric amplitude interfered with a spherical wave. Panels (d), (h), and (l) are the far field electric distribution for each metasurface.

unit groups with a constant rotation angle difference of $\pi/11$ provide 2π phase shift for the crosspolarized scattered light as shown by the red line. The arrangement of C_2 (C_3) is determined by selecting every other (three) unit cells of C_1, which is shown

at the bottom of Figure 3a, the blue (green) line reveals a larger phase conversion up to 4π (6π), representing the second order (third order) of anomalous reflection. Calculated by Equation (3), the reflection angles of the $m = 1$, 2, and 3 orders are 18.3°,

39.0°, and 70.7°, respectively. Figure 3b,d shows the simulated phase distributions of LCP light in x–z plane with perpendicularly incident RCP plane waves. The white arrows represent the direction of the incident and reflected light, respectively. The simulated reflection angles are also indicated in Figure 3b,d, which are consistent with the theoretically calculated results.

We achieved ultra-high-order anomalous reflection by reducing the response wavebands and increasing the period of super cells. Compared with traditional metasurfaces, the conductivity of graphene can be dynamically controlled by tuning the electrostatic gating. We simulated anomalous reflection spectra of a single nanocross at different Fermi energy excited by the circularly polarized light in **Figure 4**a, the rotation angle is fixed at $\varphi = 90°$. With increasing of the Fermi energy, the response waveband has a blueshift with a slight increase in reflection coefficient. We changed the number of the nanocrosses in a unit group from 4 to 7, thereby the period of super cells is increased to 46.2 μm. At the wavelength of 8.1 μm, we realized five-order anomalous reflection, and the simulated phase distribution is shown in Figure 4b, where the Fermi energy is fixed at 0.95 eV. The simulated reflection angle is in good agreement with the theoretically calculated result. Figure 4c,d shows that the metasurfaces have a strong response at the Fermi energy of 0.95 eV, however, the response basically disappears at the Fermi energy of 0.8 eV. By adjusting the gate voltage, the responses of metasurfaces can be controlled, showing a switching effect of the anomalous light. In addition, the efficiency of the output light can be dynamically controlled when gradually adjusting the gate voltage.

To validate the performance of the high-order anomalous reflection metasurfaces, we devised a series of samples with a spiral phase shift covering from 0 to $m \times 2\pi$. This particular phase distribution results in the generation of a Laguerre–Gaussian beam.[36,37] The center of the Laguerre–Gaussian beam has a helical wavefront phase singularity with an azimuthally dependent phase term, $\exp(im\varphi)$, where φ is the azimuthal angle, and m is the topological charge. Our designed metasurfaces can produce ultra-high-order anomalous vortex beam for crosspolarization light. According to the previously simulated results of the anomalous reflection, there is no coupling between the individual structural elements of the metasurfaces, and each unit cell can be simply treated as a secondary light source.[38] In order to reduce the calculation, we used MATLAB to calculate the results. Each structure is regarded as a wave source. The calculated electric field and phase distributions of vortex beam created by metasurfaces with m of 1, 3, and 15 are shown in **Figure 5**. As shown in Figure 5a, the nanocrosses are arranged with azimuthal phase shift varying from 0 to 2π, producing the first-order vortex beam. The calculated phase distribution illuminated by incident plane waves is shown in Figure 5b. Figure 5c,d shows the distributions of the electric field in the presence and absence of interfering spherical waves, respectively, which prove that a high-quality first-order vortex has been achieved. Then, we further changed the azimuthal phase of nanocrosses to cover the phase range of 6π and increased the number of samples, as shown in Figure 5e. We can clearly see the third-order vortex beam is produced from Figure 5f,g. It is worth mentioning that the divergence angle of the electric field becomes larger when increasing the

order by comparing Figure 5d,h. Using the above method, we can achieve the ultra-high-order vortex mode as long as the phase change is large enough. Figure 5i–l proves that we can numerically simulate the vortex beams in the case of $m = 15$. Its implementation greatly increases the angular momentum carried by the beam, which can be used to study the spin–orbit interaction in photonic systems and other basic physical phenomena, and can also provide a wide range of application in the optical micromanipulation. In addition, the produced vortex beam increases the information density,[39] which can be beneficial in future applications.

In summary, we proposed a novel gradient graphene metasurface, which can manipulate the wavefront of light with a broadband range in the mid-infrared regime. The metasurface works in high-order anomalous reflection modes and achieves far more than 2π phase shift conversion. As the conductivity of graphene can be dynamically controlled by electrostatic gating, not only the anomalous conversion efficiency can be maintained over a broadband range, but also the ultra-high-order mode with the dynamic control of the efficiency can be realized. Based on the gradient metareflection array, high-quality Laguerre–Gaussian beams with different orders are realized. Moreover, we achieved ultra-high-order vortex beams up to 15 orders. The high-order design obtains an additional degree of freedom, and it can provide applications in many specific physical fields, such as polarization and spectral beam splitters, high numerical aperture plasmonic lenses. With its superior performance, our design provides a wide platform for applications, such as tunable devices, information optics, polarization, and spectral beam splitters.

Conflict of Interest

The authors declare no conflict of interest.

[1] N. I. Zheludev, *Science* **2010**, *328*, 582.
[2] N. Yu, F. Capasso, *Nat. Mater.* **2014**, *13*, 139.
[3] X. Yin, Z. Ye, J. Rho, Y. Wang, X. Zhang, *Science* **2013**, *339*, 1405.
[4] J. Li, S. Chen, H. Yang, J. Li, P. Yu, H. Cheng, C. Gu, J. Tian, *Adv. Funct. Mater.* **2014**, *94*, 18.

[5] E. Almeida, G. Shalem, Y. Prior, *Nat. Commun.* **2016**, *7*, 10367.

[6] G. Li, S. Chen, N. Pholchai, B. Reineke, P. W. Wong, E. Y. Pun, K. W. Cheah, T. Zentgraf, S. Zhang, *Nat. Mater.* **2015**, *14*, 607.

[7] N. Yu, P. Genevet, M. A. Kats, F. Aieta, J. P. Tetienne, F. Capasso, Z. Gaburro, *Science* **2011**, *334*, 333.

[8] H. Mühlenbernd, P. Georgi, N. Pholchai, L. Huang, G. Li, S. Zhang, T. Zentgraf, *ACS Photonics* **2016**, *3*, 124.

[9] Y. Yang, W. Wang, P. Moitra, I. I. Kravchenko, D. P. Briggs, J. Valentine, *Nano Lett.* **2014**, *14*, 1394.

[10] W. Shu, Y. Liu, Y. Ke, X. Ling, Z. Liu, B. Huang, H. Luo, X. Yin, *Opt. Express* **2016**, *24*, 21177.

[11] W. T. Chen, M. Khorasaninejad, A. Y. Zhu, J. Oh, R. C. Devlin, A. Zaidi, F. Capasso, *Light: Sci. Appl.* **2017**, *6*, e16259.

[12] J. Zhou, Y. Liu, Y. Ke, H. Luo, S. Wen, *Opt. Lett.* **2015**, *40*, 3193.

[13] G. Li, M. Kang, S. Chen, S. Zhang, E. Y.-B. Pun, K. W. Cheah, J. Li, *Nano Lett.* **2013**, *13*, 4148.

[14] H. Cheng, S. Chen, P. Yu, W. Liu, Z. Li, J. Li, B. Xie, J. Tian, *Adv. Opt. Mater.* **2015**, *3*, 1744.

[15] Y. Fan, N.-H. Shen, F. Zhang, Z. Wei, H. Li, Q. Zhao, Q. Fu, P. Zhang, T. Koschny, C. M. Soukoulis, *Adv. Opt. Mater.* **2016**, *4*, 1824.

[16] J. Li, P. Yu, H. Cheng, W. Liu, Z. Li, B. Xie, S. Chen, J. Tian, *Adv. Opt. Mater.* **2016**, *4*, 91.

[17] Z. Li, J. Hao, L. Huang, H. Li, H. Xu, Y. Sun, N. Dai, *Opt. Express* **2016**, *24*, 8788.

[18] H. Cheng, S. Chen, P. Yu, J. Li, L. Deng, J. Tian, *Opt. Lett.* **2013**, *38*, 1567.

[19] C. Luo, D. Li, J. Yao, F. Ling, *J. Electromagn. Waves Appl.* **2015**, *29*, 2512.

[20] V. Yachin, L. Ivzhenko, S. Polevoy, S. Tarapov, *Appl. Phys. Lett.* **2016**, *109*, 221905.

[21] F. H. L. Koppens, D. E. Chang, F. J. G. de Abajo, *Nano Lett.* **2011**, *11*, 3370.

[22] N. Dabidian, S. Dutta-Gupta, I. Kholmanov, K. Lai, F. Lu, J. Lee, M. Jin, S. Trendafilov, A. Khanikaev, B. Fallahazad, E. Tutuc, M. A. Belkin, G. Shvets, *Nano Lett.* **2016**, *16*, 3607.

[23] V. W. Brar, M. S. Jang, M. Sherrott, J. J. Lopez, H. A. Atwater, *Nano Lett.* **2013**, *13*, 2541.

[24] Y. Fan, Z. Wei, Z. Zhang, H. Li, *Opt. Lett.* **2013**, *38*, 5410.

[25] Q. Li, L. Cong, R. Singh, N. Xu, W. Cao, X. Zhang, Z. Tian, L. Du, J. Han, W. Zhang, *Nanoscale* **2016**, *8*, 17278.

[26] Y. Zhang, T. Li, Q. Chen, H. Zhang, J. F. O'Hara, E. Abele, A. J. Taylor, H. Chen, A. K. Azad, *Sci. Rep.* **2015**, *5*, 18463.

[27] Z. Li, G. Zheng, P. He, S. Li, Q. Deng, J. Zhao, Y. Ai, *Opt. Lett.* **2015**, *40*, 4285.

[28] F. Aieta, P. Genevet, M. A. Kats, N. Yu, R. Blanchard, Z. Gaburro, F. Capasso, *Nano Lett.* **2012**, *12*, 4932.

[29] X. Chen, L. Huang, H. Mühlenbernd, G. Li, B. Bai, Q. Tan, G. Jin, C. Qiu, S. Zhang, T. Zentgraf, *Nat. Commun.* **2012**, *3*, 1198.

[30] S. Larouche, D. R. Smith, *Opt. Lett.* **2012**, *37*, 2391.

[31] E. Palik, G. Ghosh, *Handbook of Optical Constants of Solids*, Academic Press, Orlando, FL **1985**.

[32] B. J. Kim, H. Jang, S.-K. Lee, B. H. Hong, J.-H. Ahn, J. H. Cho, *Nano Lett.* **2010**, *10*, 3464.

[33] Y. Cui, C. Zeng, *J. Appl. Phys.* **2017**, *121*, 143102.

[34] Z. Fang, S. Thongrattanasiri, A. Schlather, Z. Liu, L. Ma, Y. Wang, P. M. Ajayan, P. Nordlander, N. J. Halas, F. J. G. de Abajo, *ACS Nano* **2013**, *7*, 2388.

[35] *COMSOL Multiphysics User's Guide, Version number 4.3*, Comsol AB, Burlington, MA, USA **2012**.

[36] E. Maguid, I. Yulevich, D. Veksler, V. Kleiner, M. L. Brongersma, E. Hasman, *Science* **2016**, *352*, 1202.

[37] Y. He, Z. Liu, Y. Liu, J. Zhou, Y. Ke, H. Luo, S. Wen, *Opt. Lett.* **2015**, *40*, 5506.

[38] C. Pfeiffer, A. Grbic, *Phys. Rev. Lett.* **2013**, *110*, 197401.

[39] Z. Bouchal, R. Celechovský, *New J. Phys.* **2004**, *6*, 131.